

Comments and Corrections

Corrections to “Silicon-Based On-chip Electrically-Tunable Spectral Shaper for Continuously Tunable Linearly Chirped Microwave Waveform Generation”

Weifeng Zhang, *Student Member, IEEE*, and Jianping Yao, *Fellow, IEEE, Fellow, OSA*

In the above paper [1], it was mistakenly printed without the Invited Paper heading. This is an invited paper for the 2016 Special Issue on Microwave Photonics.

[1] W. Zhang and J. Yao, “Silicon-based on-chip electrically-tunable spectral shaper for continuously tunable linearly chirped microwave waveform generation,” *J. Lightw. Technol.*, vol. 34, no. 20, pp. 4664–4672, Oct. 2016.

Silicon-Based On-Chip Electrically-Tunable Spectral Shaper for Continuously Tunable Linearly Chirped Microwave Waveform Generation

Weifeng Zhang, *Student Member, IEEE*, and Jianping Yao, *Fellow, IEEE, Fellow, OSA*

Abstract—A silicon-based on-chip electrically-tunable spectral shaper for the generation of a tunable linearly chirped microwave waveform (LCMW) based on spectral shaping and wavelength-to-time (SS-WTT) mapping is designed, fabricated, and demonstrated. The on-chip spectral shaper has a Michelson interferometer structure with two linearly chirped waveguide Bragg gratings (LC-WBGs) incorporated in its two arms. Due to the wavelength-dependent length difference between the two arms of the interferometer, the spectral response of the spectral shaper exhibits a wavelength-dependent free spectral range, which is required for the generation of an LCMW based on SS-WTT mapping. To enable electrical tuning of the spectral response, a lateral PN junction is introduced to each of the waveguides where the LC-WBGs are inscribed. Thanks to the plasma dispersion effect, the spectral response of the spectral shaper can be tuned by changing the bias voltages applied to the PN junctions, which would lead to the tuning of the generated LCMW. A theoretical analysis on the LCMW generation is performed, which is verified by an experiment in which an electrically-tunable spectral shaper is fabricated using a CMOS-compatible process with 248-nm deep ultraviolet lithography. By independently controlling the bias voltages to the PN junctions, a continuous tuning of the generated LCMW is demonstrated.

Index Terms—Linearly chirped microwave waveform (LCMW), linearly chirped waveguide grating (LC-WBG), microwave photonics, optical pulse shaping, silicon photonics, wavelength-to-time mapping.

I. INTRODUCTION

A linearly chirped microwave waveform (LCMW) with a large time bandwidth product (TBWP) is widely used in modern radar systems to enhance the range resolution [1]. To provide a better resolution, an LCMW with a central frequency up to tens or even hundreds of gigahertz and a bandwidth of a few gigahertz is required [2]. However, limited by the speed of an electronic analog-to-digital converter, an LCMW generated using a digital circuit falls short of meeting the need of high frequency and wide bandwidth [3]–[4]. To fulfill the need, photonic techniques have been studied for the generation of

high frequency and wideband LCMWs for the last few years, thanks to the key advantage of the high frequency and the broad bandwidth offered by modern photonics [5]–[10]. In addition, with the development of multifunctional radar systems, more stringent requirements are imposed on the microwave waveforms. For example, it is desired that the central frequency or the chirp rate of an LCMW can be tuned to maximize the performance of a radar system. Therefore, the tuning of an LCMW is practically needed. Among the numerous techniques for photonic-assisted microwave waveform generation, spectral shaping and wavelength-to-time (SS-WTT) mapping is considered a technique with good simplicity and flexibility, and has been extensively researched [11]. In an SS-WTT system, the tuning of the generated microwave waveform is done by changing the spectral response of the spectral shaper [11], which can be implemented by using a tunable optical filter serving as the spectral shaper.

A fiber interferometer is an optical filter which was employed as a spectral shaper in [12] to demonstrate the tuning in the central frequency and chirp rate of an LCMW. By tuning the dispersion unbalance or the relative delay between the two arms of the interferometer, the spectral response with tunable free-spectral range (FSR) was achieved, which led to the generation of an LCMW with a tunable chirp rate or a tunable central frequency. In [12], an LCMW with a central frequency ranging from 100 MHz to 25 GHz and a chirp rate ranging from -160 to $+160$ MHz/ns was experimentally generated. However, the TBWP of the generated microwave waveform is quite small, which is ~ 12 . This small TBWP is due to the narrow bandwidth of the linearly chirped fiber Bragg grating (LC-FBG) used to perform WTT mapping, which limits the entire bandwidth of the SS-WTT system. In addition, the tuning of the central frequency was done by changing the length difference between the two arms in the interferometer using a tunable delay line. To simplify the frequency tuning, we proposed to use an optically pumped LC-FBG written in an erbium–ytterbium co-doped fiber. By incorporating such an LC-FBG in one arm of the interferometer, the central frequency of the generated LCMW can be tuned through optical pumping [13]. Again, the TBWP of the generated LCMW is small, which is ~ 24.5 . The small TBWP is again due to the small bandwidth of the optically pumped LC-FBG. In [14], instead of using an optically pumped LC-FBG, a reconfigurable pulse shaper with a much wider bandwidth was incorporated in one arm of a fiber interferometer, an LCMW with a large TBWP of 589 was experimentally generated. However, all the approaches reported in [12]–[14] were implemented

Manuscript received February 21, 2016; revised May 14, 2016; accepted May 24, 2016. Date of publication May 26, 2016; date of current version September 25, 2016. This work was supported in part by the Natural Science and Engineering Research Council of Canada through the Silicon Electronic-Photonic Integrated Circuits CREATE program and the CMC Microsystems.

The authors are with the Microwave Photonics Research Laboratory, School of Electrical Engineering and Computer Sciences, University of Ottawa, ON K1N 6N5, Canada (e-mail: jpyao@eecs.uOttawa.ca)

Color versions of one or more of the figures in this paper are available online at <http://ieeexplore.ieee.org>.

Digital Object Identifier 10.1109/JLT.2016.2574125

based on fiber optics, which makes the system a large size and a poor stability.

To overcome the inherent disadvantages of a fiber-optics based system, it is desirable that a waveform generation system is implemented based on photonic integrated circuits [15]–[16]. For example, a chip-level optical spectral shaper was proposed and demonstrated for LCMW generation [17]. The spectral shaper was implemented based on a silicon chip consisting of multiple cascaded microring resonators. By thermally tuning the microring resonators, the spectral response of the spectral shaper was changed, which led to the change in the generated LCMW. In the experimental demonstration, an LCMW with a central frequency of 8 GHz and a TBWP of ~ 12 was demonstrated. Due to the limited thermal-tuning range, the generated LCMW has a small chirp rate, which led to a small bandwidth as well as a small TBWP.

To generate an LCMW with a large TBWP, recently we have designed a novel silicon-based on-chip optical spectral shaper and demonstrated the photonic generation of an LCMW [18]–[19]. The on-chip optical spectral shaper has a Mach-Zehnder interferometer (MZI) structure with two identical linearly chirped waveguide gratings (LC-WBGs) having complementary chirp rates that are incorporated in the two arms. It is different from an LC-FBG where the chirp is produced by continuously changing the period along the grating, here in an LC-WBG the chirp is realized by linearly varying the rib width along the grating while maintain the corrugations on the slab waveguide sidewall uniform. An offset waveguide is added in one arm of the MZI to introduce a length difference between the two arms. Depending on the length of the offset waveguide, the spectral shaper could have a spectral response with a symmetrical, a uniformly increasing or decreasing FSR. LCMWs with different central frequencies and large TBWPs (as large as 615) were generated. However, using the system in [18]–[19], an LCMW could not be tuned since the spectral response of the spectral shaper is fixed once the spectral shaper is fabricated, which makes the system only suitable for the generation of a pre-designed microwave waveform. For many applications, tunable LCMWs are needed.

In this paper, a silicon-based on-chip electrically-tunable spectral shaper is designed and fabricated, and is used for the generation of tunable LCMWs based on SS-WTT mapping. The on-chip spectral shaper has a Michelson interferometer structure with two LC-WBGs having the complementary chirp rates incorporated in its two arms. The spectral response of the spectral shaper exhibits a wavelength-dependent FSR, which is required for the generation of an LCMW based on SS-WTT mapping. To enable the spectral shaper to have an electrically-tunable spectral response, a lateral PN junction is introduced to the waveguide where an LC-WBG is inscribed. Due to the plasma dispersion effect, the refractive index of the waveguide is changed when the bias voltage applied to the PN junction is changed, which lead to the tuning of the spectral response of the LC-WBG. By incorporating the two electrically-tunable LC-WBGs in the two arms, the spectral shaper could be electrically tuned. A theoretical analysis is performed which is validated by an experiment

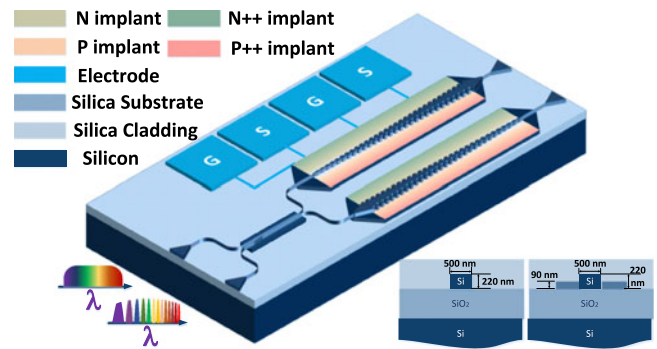


Fig. 1. Perspective view of the proposed silicon-based on-chip electrically-tunable optical spectral shaper.

using an electrically-tunable spectral shaper that is fabricated using a CMOS-compatible process with 248-nm deep ultraviolet lithography. By independently controlling the bias voltages to the PN junctions, a continuous tuning of a generated LCMW is demonstrated. The key advantage of the proposed spectral shaper is its ultra-fast tunability, which is enabled by the plasma dispersion effect in silicon.

II. SPECTRAL SHAPER DESIGN AND MEASUREMENT

Fig. 1 illustrates the perspective view of the proposed electrically-tunable spectral shaper, and the inset shows the fundamental waveguide structures of a strip waveguide and a rib waveguide used in the spectral shaper. To minimize the chip footprint, the strip waveguide is used to guide the light, while the rib waveguide is employed for the LC-WBG where a lateral PN junction is made to achieve electrical tunability. To ensure a single transverse-electric (TE) mode operation, the strip waveguide is designed to have a width of 500 nm and a height of 220 nm, and the rib waveguide is designed to have a width of 500 nm, a height of 220 nm, and a slab thickness of 90 nm. Since the structures of the two waveguides are different, a double-layer linear taper waveguide is required to achieve the mode transition between the two waveguides. Fig. 2(a) presents the schematic layout of an electrically-tunable spectral shaper, which has a Michelson interferometer structure consisting of a directional coupler [20] and a pair of electrically-tunable LC-WBGs with independent bias contacts. A TE-mode grating coupler [21] is used to couple the light into the chip through port 1 of the directional coupler. After the directional coupler, the input light is equally split and the split light waves are sent to the LC-WBGs with complementary chirp rates. The spectral components of the light waves at different wavelengths are reflected from different positions along the LC-WBGs and are recombined at directional coupler. Using another grating coupler, the combined light wave is coupled out of the chip. Thanks to the wavelength-dependent length difference between the two arms of the interferometer, the spectral shaper exhibits a wavelength-dependent FSR, which is required for the generation of an LCMW based on the SS-WTT mapping. In order to realize independently electrical tuning of each of the LC-

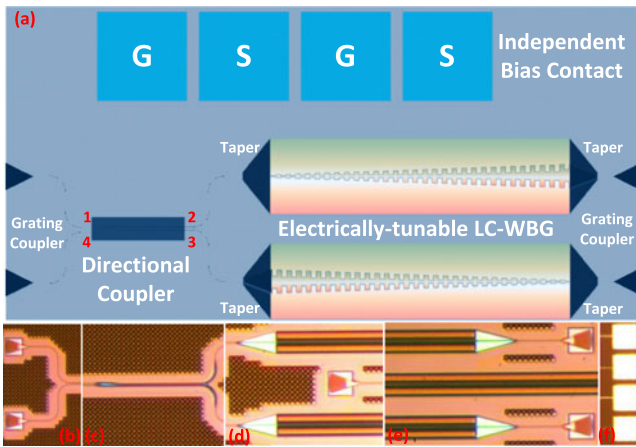


Fig. 2. (a) Schematic layout of the designed electrically-tunable spectral shaper; (b) photograph of the input and output grating couplers, (c) photograph of the 2×2 adiabatic 3-dB directional coupler, (d) photograph of the front of the LC-WBGs, (e) photograph of the end of the LC-WBGs, (f) photograph of the two pairs of the bias contacts in the fabricated electrically-tunable spectral shaper.

WBGs, two pairs of the bias contacts are designed and implemented. Note that at the right end of each of the LC-WBGs, a grating coupler is used as a waveguide terminator to avoid unwanted reflections. To achieve the mode transition between a strip waveguide and a rib waveguide, a taper with a length of $50 \mu\text{m}$ is added before and after the LC-WBGs. Fig. 2(b) is a photograph of the input and output grating couplers for light coupling between the fiber and the chip in the fabricated spectral shaper, captured by a microscope camera. Their center-to-center spacing is $127 \mu\text{m}$, which matches the spacing of the fiber array used for the experiment. Fig. 2(c) is a photograph of the 2×2 adiabatic 3-dB directional coupler. Fig. 2(d) is a photograph of the front of the LC-WBGs, and Fig. 2(e) is a photograph of the end of the LC-WBGs. Note that the tapers are also shown in the two photographs in Figs. 2(d) and (e), and the grating coupler as a terminator is shown in Fig. 2(e). Fig. 2(f) shows a photograph of the two pairs of the bias contacts. A contact has a dimension of $80 \times 80 (\mu\text{m} \times \mu\text{m})$ and the center-to-center spacing between two contacts is $100 \mu\text{m}$.

An electrically-tunable LC-WBG is a key component in realizing the proposed electrically-tunable spectral shaper. Fig. 3(a) presents the top view of an electrically-tunable LC-WBG. In [19], we reported an LC-WBG, which was fabricated on a rib waveguide in which periodic corrugations were introduced to the sidewalls of the slab waveguide and the chirp was achieved by linearly increasing the rib width along the gratings. To use the plasma dispersion effect in silicon to realize electrical tunability, however, the corrugations have to be moved to the sidewalls of the rib waveguide. To effectively suppress the sidelobes in the reflection spectral response, Gaussian apodization, a technique to tailor the grating spectral response to reduce the ripples, is applied to the grating, which is done by varying the corrugation depths in a raised Gaussian profile along the rib waveguide. To enable the grating to work in C band, the grating period is designed to be 310 nm with a duty cycle of 50%, correspond-

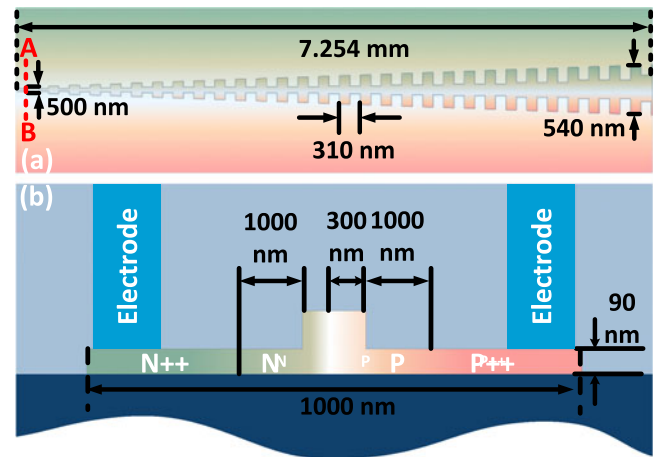


Fig. 3 (a) Top-view of the electrically-tunable LC-WBG and (b) cross-sectional view of the electrically-tunable LC-WBG along the line AB.

ing to a Bragg wavelength of 1550 nm , and the rib width is increasing linearly from 500 to 540 nm . The total length of the grating is 7.254 mm with an expected time delay of 170 ps . Fig. 3(b) presents the cross-sectional view of the electrically-tunable LC-WBG along the line AB in Fig. 3(a). An asymmetrical lateral PN junction is employed, which is slightly shifted to the left from the center of the waveguide by 50 nm . Such a shift could increase the mode overlap with the p-type doping region to achieve a higher tuning efficiency, since the plasma dispersion effect is more sensitive to the change of the free-hole concentration. Additional p++ and n++ implantations, $1 \mu\text{m}$ away from the rib to minimize absorption losses, are utilized for ohmic contact formation. Two contact windows are opened on the silica pads, with a $2\text{-}\mu\text{m}$ -thick aluminum layer deposited to make the ohmic contacts.

The electrically-tunable LC-WBG is fabricated using the CMOS-compatible process with 248-nm deep ultraviolet lithography at IME, Singapore. The optical performance of the fabricated electrically-tunable LC-WBG is evaluated using an optical vector analyzer (LUNA OVA CTe). Figs. 4(a) and (b) shows, respectively, the normalized reflection spectral and the group delay responses of the LC-WBG when biased at 0 V , $+20 \text{ V}$ and -1.0 V . When the bias voltage is zero, as shown in Fig. 4(b) in red, the grating exhibits a time delay of 174.9 ps between 1529.14 and 1538.77 nm and thus has a dispersion value of 18.161 ps/nm and a chirp rate of 1.328 nm/mm . It is apparent to see from Fig 4(a) that the grating has a comparatively large insertion loss at the longer wavelength. This is because the light wave with a longer wavelength needs to travel a longer distance in the LC-WBG until it is reflected at the right location of the LC-WBG, since the rib width is linearly increasing along the grating. The loss includes the grating-induced loss and the doping-induced loss. When the grating is forward biased at -1.0 V , as shown in Fig. 4(b) in blue, the grating exhibits a time delay of 124.10 ps between 1529.10 and 1536.00 nm and thus has a dispersion value of 17.938 ps/nm and a chirp rate of 0.951 nm/mm . It is worth noting that the spectrum is slightly blue-shifted compared

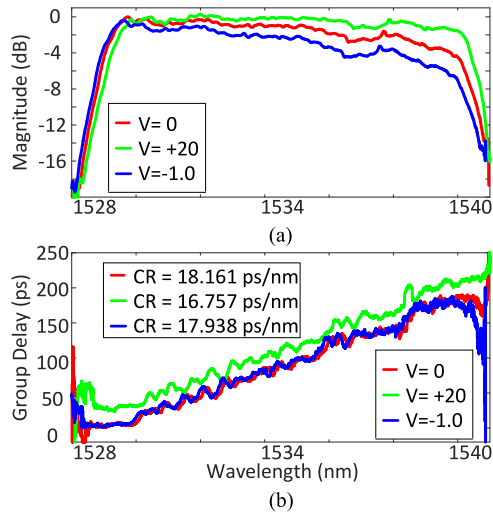


Fig. 4. (a) Measured spectral and (b) group delay responses of a fabricated electrically-tunable LC-WBG under the different bias voltages.

to the spectrum when no bias voltage is applied. For forward biasing, when the bias voltage is increasing, the free-carrier injection would decrease the refractive index due to the plasma dispersion effect, which leads to a blue shift in the spectrum. In the meanwhile, the increased free-carrier density would also introduce an excess absorption loss. Therefore, the blue line exhibits a clearly changing insertion loss for different wavelengths. When the grating is reversed biased at +20 V, as shown in Fig. 4(b) in green, the grating exhibits a time delay of 182.27 ps between 1529.36 and 1540.24 nm and thus has a dispersion value of 16.757 ps/nm and a chirp rate of 1.500 nm/mm. Again a red-shift in the spectrum is observed. For reverse biasing, when the bias voltage is increasing, the free-carrier extraction would increase the refractive index via plasma dispersion effect, which leads to a red shift in the spectrum. Furthermore, since the free-carrier density is decreased, the doping-induced loss is decreased, which would alleviate the insertion loss difference for the light wave at different wavelengths. As can be found in Fig. 4, the magnitude and group delay responses of the LC-WBG could be tuned by controlling the bias voltage, which will be used in the proposed spectral shaper for spectral response tuning. Note that the ripples in the magnitude and the group delay responses are high, which are mainly caused by the fabrication limitations since the line width of the corrugations is smaller than the feature size [22]. To reduce the ripples, advanced fabrication process should be used, in which the feature size should be smaller than the minimum line width of the LC-WBG. In addition, by applying apodization to the grating during the design and fabrication, the ripples could also be reduced.

Then, the optical performance of the fabricated electrically-tunable spectral shaper is evaluated. The on-chip spectral shaper has a Michelson interferometer structure, in which two identical electrically-tunable LC-WBGs with complementary chirp rates are incorporated in the two arms. The total length of the LC-WBG is designed to be 7.0 mm. In the LC-WBG, the rib width is linearly increasing from 500 to 540 nm and Gaussian apodization is employed by varying the corrugation depth in a

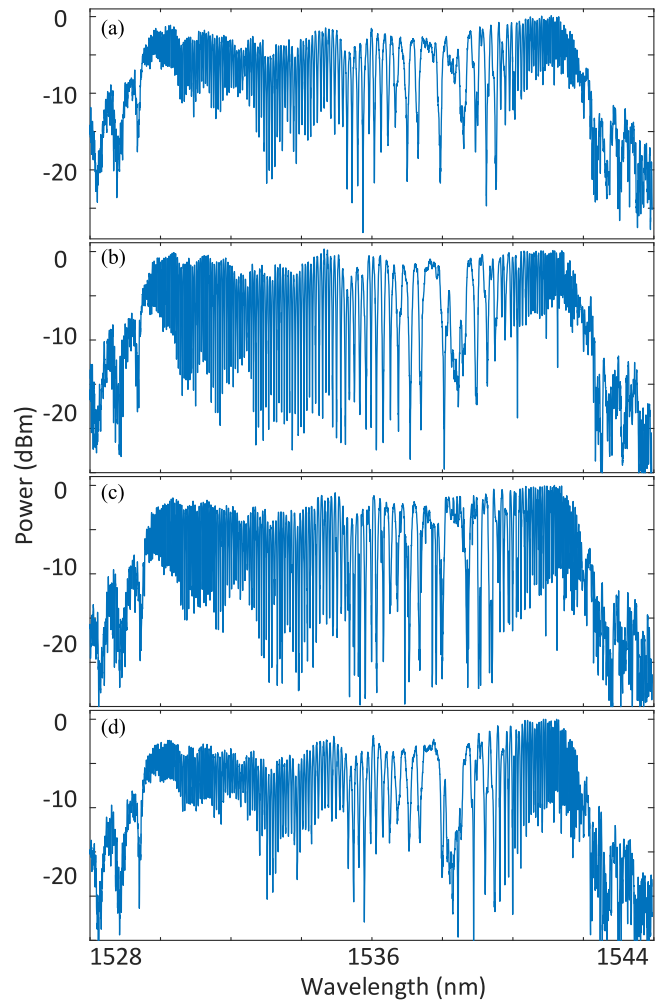


Fig. 5. Measured spectral responses of the fabricated spectral shaper when (a) no bias voltage is applied; (b) a reverse-biased voltage of +20 V is applied to the LC-WBG in the upper arm; (c) two identical reverse-biased voltages of +20 V are applied to the LC-WBGs in both arms; (d) a reverse-biased voltage of +20 V is applied to the LC-WBG in the upper arm while a forward-biased voltage of -1.0 V is applied to the LC-WBG in the lower arm;

raised Gaussian profile along the grating. The entire electrically-tunable spectral shaper has a size of 7.10 mm in length and 0.016 mm in width, giving a small footprint of 0.114 mm².

Fig. 5(a) shows the measured spectral response of the fabricated spectral shaper when no bias voltage is applied. Since the spectral shaper has a symmetric configuration, the spectral response presents a symmetrically varying FSR. Note that the measured spectral response in Fig. 5(a) is slightly asymmetrical, which is caused by the Gaussian apodization applied to the grating.

Fig. 5(b) shows a measured spectral response of the fabricated spectral shaper when a reverse-biased voltage of +20 V is applied to the LC-WBG in the upper arm. Since there is no bias voltage applied to the LC-WBG in the lower arm, its reflection spectrum is kept unchanged, while the spectrum of the LC-WBG in the upper arm when reverse biased would be red-shifted, which would finally lead to a change in the spectral response of the spectral shaper.

Fig. 5(c) shows the measured spectral response of the fabricated spectral shaper when two identical reverse-biased voltages of +20 V are applied to the LC-WBGs in both arms. Since the spectrums of the two LC-WBGs are both red-shifted, there would be a double change in the spectral response of the spectral shaper.

Fig. 5(d) shows the spectrum of the spectral shaper when a reverse-biased voltage of +20 V is applied to the LC-WBG in the upper arm and a forward-biased voltage of -1.0 V is applied to the LC-WBG in the lower arm. The spectrum of the LC-WBG in the upper arm is red-shifted, and that of the LC-WBG in the lower arm is blue-shifted, which would cause a change in the spectral response of the spectral shaper. As can be seen in Fig. 5, by independently tuning bias voltages applied to the two LC-WBGs, the spectral shaper would exhibit a tunable spectral response, which would lead to the generation of a tunable LCMW.

Note that the insertion loss of the fabricated spectral shaper is measured to be around 24 dB, which is mainly resulted from the fiber-to-fiber coupling loss and the splitting loss of the directional coupler.

III. PRINCIPLE OF WAVEFORM GENERATION

In a typical SS-MTT mapping system for LCMW generation, an ultra-short optical pulse from a mode-locked laser is launched into the spectral shaper to generate a spectrally shaped optical pulse with the spectrum identical to shape of the microwave waveform. By passing the spectrally-shaped optical pulse through a dispersive element such as a dispersion compensating fiber (DCF), linear WTT mapping is performed, and a microwave waveform with a shape identical the shaped spectrum is generated at the output of a photodetector (PD). The fundamental principle is identical to the one reported by us in [19] except the chirp rates of the two LC-WBGs in our proposed spectral shaper could be independently tuned by applying a bias voltage, which enables the system to have a largely flexible tunability.

Based on the analysis in [19], the instantaneous microwave carrier frequency of the generated microwave waveform can be expressed as

$$f_{\text{RF}}(\delta t) = \frac{2}{\lambda_0^2} \frac{n_{\text{eff}0} \Delta L_0}{\ddot{\Phi}_\lambda} + \frac{2}{\lambda_0^2} \frac{n_{\text{eff}1} \delta t}{C_1 \ddot{\Phi}_\lambda^2} - \frac{2}{\lambda_0^2} \frac{n_{\text{eff}2} \delta t}{C_2 \ddot{\Phi}_\lambda^2} \quad (1)$$

where λ_0 is the center wavelength of the input optical pulse, δt (nm) is the time detuning from the center of the temporal waveform, C_1 (nm/mm) and C_2 (nm/mm) are the chirp rates of the LC-WBGs in the upper and lower arms, respectively, $n_{\text{eff}1}$ and $n_{\text{eff}2}$ are the average effective refractive indices of the LC-WBGs in the upper and lower arms, respectively, $\ddot{\Phi}_\lambda$ is the group velocity dispersion (GVD) of the dispersive element, and ΔL_0 is the length difference between the two arms of the spectral shaper. Since the proposed spectral shaper has a symmetrical configuration, ΔL_0 is equal to zero. For the two LC-WBGs have complementary chirp rates, C_1 is positive and C_2 is negative.

Then, the equation could be rewritten as

$$f_{\text{RF}}(\delta t) = \frac{2}{\lambda_0^2} \frac{n_{\text{eff}1} \delta t}{C_1 \ddot{\Phi}_\lambda^2} - \frac{2}{\lambda_0^2} \frac{n_{\text{eff}2} \delta t}{C_2 \ddot{\Phi}_\lambda^2} \quad (2)$$

which shows that the instantaneous microwave frequency of the generated microwave waveform is linear with time and dependent on the chirp rates of the two LC-WBGs for a given dispersive element for WTT mapping. Thanks to the electrical tunability of the LC-WBGs in the spectral shaper, the instantaneous microwave frequency of the generated microwave waveform could be tuned by tuning the bias voltages to the LC-WBGs.

In addition, according to (2), for a dispersive element with a given dispersion, the central frequency of the generated chirped microwave waveform is zero when $\delta t = 0$ and is independent of the chirp rates of the LC-WBGs. When the chirp rate of an LC-WBG or the chirp rates of the two LC-WBGs are varied by changing the applied bias voltages, the central frequency of the generated chirped microwave waveform is still kept zero. To have a non-zero central frequency, an offset waveguide can be added in one arm to introduce a length difference between the two arms. With the different length difference between the two arms, the central frequency of the generated chirped microwave waveform could be different.

The chirp rate of the generated microwave waveform is given by

$$CR = \frac{df_{\text{RF}}(\delta t)}{dt} = \frac{2}{\lambda_0^2} \frac{n_{\text{eff}1}}{C_1 \ddot{\Phi}_\lambda^2} - \frac{2}{\lambda_0^2} \frac{n_{\text{eff}2}}{C_2 \ddot{\Phi}_\lambda^2} \quad (3)$$

which is determined by the chirp rates of the two LC-WBGs for a dispersive element with a given dispersion. Again, the chirp rate of the generated microwave waveform could be tuned by tuning the applied bias voltages to the LC-WBGs.

The pulse compression ratio is determined by the TBWP of the generated microwave waveform. In our system, the TBWP of the generated chirped microwave waveform is calculated by

$$TBWP = CR \cdot \Delta T^2 = \left(\frac{2}{\lambda_0^2} \frac{n_{\text{eff}1}}{C_1} - \frac{2}{\lambda_0^2} \frac{n_{\text{eff}2}}{C_2} \right) B_\lambda^2 \quad (4)$$

where B_λ is the spectral width of the input optical pulse since the bandwidth of the spectral shaper is broader than the spectral width of the optical pulse. It can be found that the TBWP is independent of the dispersion of the dispersive element but determined by the chirp rates of the LC-WBGs and the spectral width of the input optical pulse. For a given input optical pulse with the spectral width of B_λ , by varying the bias voltages to the LC-WBGs, the chirp rates are changed, which leads to a change in the TBWP. Compared with a fiber-based spectral shaper, our proposed spectral shaper has a comparatively large spectral bandwidth, thanks to the strong index modulation in the LC-WBGs, which enables the system to generate an LCMW generation with a comparatively large TBWP.

IV. EXPERIMENT

Fig. 6(a) shows the experimental setup. An optical Gaussian pulse train from a mode-lock laser (MLL) (Pritel 1550-nm

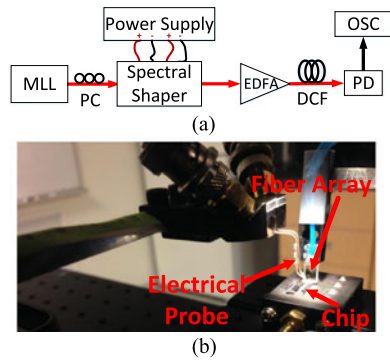


Fig. 6. (a). Experimental setup. MML: mode lock laser. PC: polarization controller. EDFA: erbium-doped fiber amplifier. DCF: dispersion compensating fiber. PD: photodetector. OSC: oscilloscope. (b) Image of the fiber array and electrical probe applied on the chip captured by a camera.

Picosecond and Femtosecond Fiber Lasers) with a pulse duration of approximately 600 fs, a spectral width of 8 nm, and a repetition rate of 40 MHz, is launched into the on-chip spectral shaper via a polarization controller (PC). The PC is used to adjust the state of polarization of the input optical pulse to minimize the polarization-dependent loss. At the output of the spectral shaper, a spectrally-shaped optical pulse is generated, which is amplified by an EDFA and then sent to a DCF with a GVD of -1020 ps/nm serving as a dispersive element to perform WTT mapping. The optical waveform at the output of the DCF is applied to a PD (NewFocus Model 1014, 45 GHz bandwidth). An LCMW is generated at the output of the PD, which is monitored using a sampling oscilloscope (OSC, Agilent 86116A, 63 GHz bandwidth). Two independent bias voltages from a power supply are applied to the two LC-WBGs to achieve waveform tuning. Fig. 6(b) is a photograph captured by a camera which presents a fiber array for the light coupling into and out of the chip and a pair of electrical probes for the bias voltages.

An experiment is performed to generate a tunable LCMW using the fabricated electrically-tunable spectral shaper.

First, two bias voltages are kept zero. Fig. 7(a) shows the temporal waveform of the generated LCMW. As can be seen, the generated LCMW has a temporal duration of around 7.95 ns. Fig. 7(b) presents its spectrogram that exhibits a symmetrical chirp profile, which matches the spectral response of the fabricated spectral shaper. Its central frequency is 0.80 GHz, which is slightly different from the theoretical value of 0 GHz. This non-zero value is resulted from a small asymmetry between the two arms of the spectral shaper induced by fabrication imperfections. On the right side of the center, the instantaneous frequency is linearly increasing with a positive chirp rate of 2.96 GHz/ns, which agrees well with a theoretical value of 3.21GHz/ns by (7). On the left side of the center, the instantaneous frequency is linearly decreasing with a negative chirp rate of -6.25 GHz/ns. The difference in the chirp rate is due to the asymmetry of the two LC-WBGs in the two arms of the MZI, which is caused by Gaussian apodization. From the time-domain waveform and its carrier frequency distribution, the TBWP of the generated LCMW is estimated to be around 133.8. Fig. 7(c) shows a compressed pulse with a pulse width of 40 ps, which is obtained

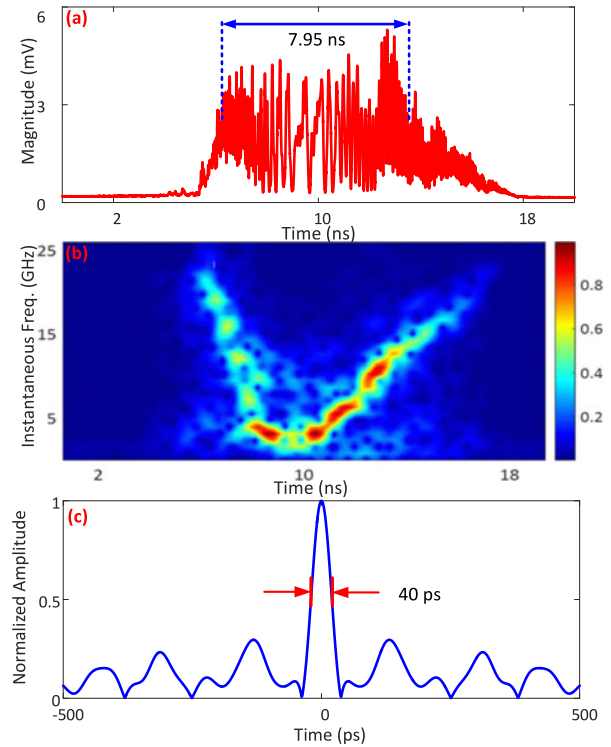


Fig. 7. Experimental results: (a) the generated LCMW; (b) the spectrogram and instantaneous frequency of the generated LCMW, and (c) the compressed pulse by autocorrelation.

by calculating the autocorrelation of the generated microwave waveform. Note that the direct-current component in the generated LCMW is removed before calculating the autocorrelation. By comparing the pulse width of the waveforms in Figs. 7(a) and (c), a pulse compression ratio as large as 198.8 is obtained.

Second, a bias voltage of $+20$ V is applied to the LC-WBG in the upper arm only. Fig. 8(a) shows the temporal waveform of the generated LCMW. As can be seen, the generated LCMW has a temporal duration of around 9.15 ns. Fig. 8(b) presents its spectrogram which exhibits a symmetrical chirp profile. Its central frequency is 0.14 GHz, closer to a theoretical value of 0 GHz. On the right side of the center, the instantaneous frequency is linearly increasing with a positive chirp rate of 2.68 GHz/ns. On the left side of the center, the instantaneous frequency is linearly decreasing with a negative chirp rate of -6.10 GHz/ns. Smaller chirp rates are expected based on (3). A larger chirp rate of a LC-WBG, a smaller chirp rate of a generated LCMW. Since the LC-WBG is reverse biased, its chirp rate is increased, which leads to the decrease in the chirp rate of the generated LCMW. Based on Fig. 8(b), the TBWP of the generated LCMW is estimated to be around 125.0. According to (4), a smaller chirp rate of the LC-WBG results in a greater TBWP of the generated LCMW. Fig. 8(c) shows the compressed pulse with a pulse width of 42 ps. By comparing the temporal widths of the waveforms in Fig. 8(a) and (c), a pulse compression ratio as large as 181.9 is obtained.

Then, two identical biased voltages of $+20$ V are applied to the LC-WBGs in both arms. Fig. 9(a) shows the temporal waveform of the generated LCMW. As can be seen, the generated

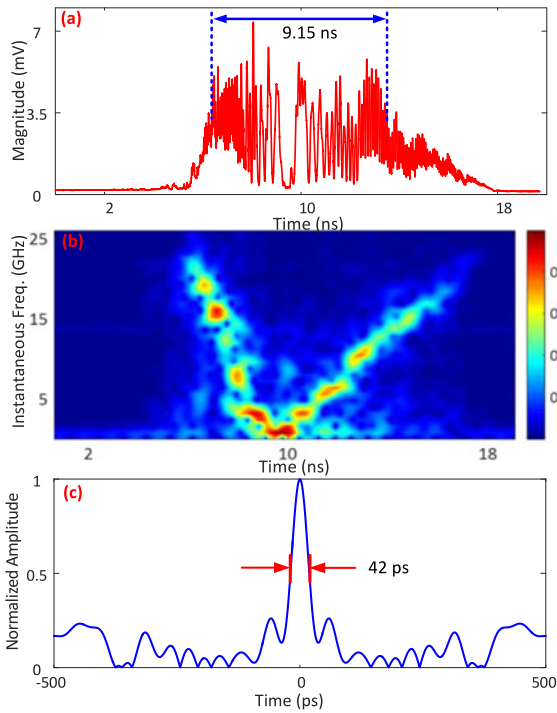


Fig. 8. Experimental results: (a) the generated LCMW; (b) the spectrogram and instantaneous frequency of the generated LCMW, and (c) the compressed pulse by autocorrelation.

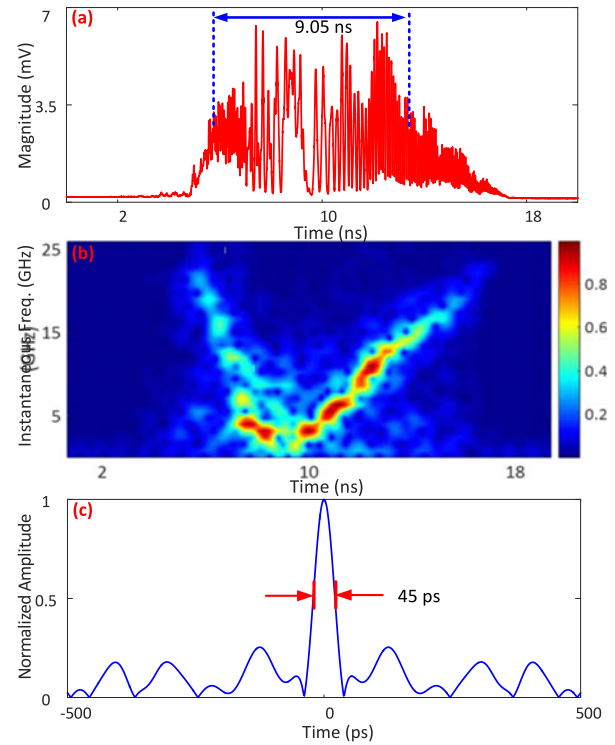


Fig. 10. Experimental results: (a) the generated LCMW; (b) the spectrogram and instantaneous frequency of the generated LCMW, and (c) the compressed pulse by autocorrelation.

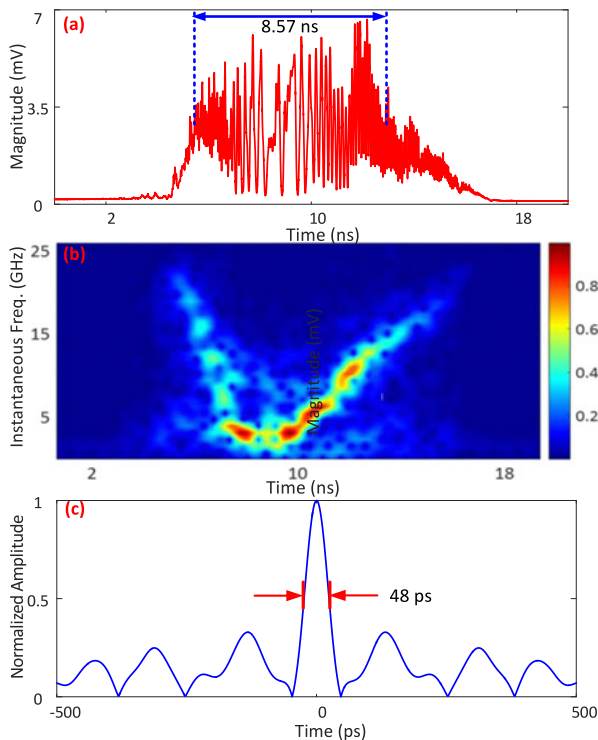


Fig. 9. Experimental results: (a) the generated LCMW; (b) the spectrogram and instantaneous frequency of the generated LCMW, and (c) the compressed pulse by autocorrelation.

LCMW has a temporal duration of around 8.57 ns. Fig. 9(b) presents its spectrogram which exhibits a symmetrical chirp profile and a central frequency of 0.73 GHz. On the right side of the center, the instantaneous frequency is linearly increasing with a positive chirp rate of 2.51 GHz/ns, and on the left side of the center, the instantaneous frequency is linearly decreasing with a negative chirp rate of -5.84 GHz/ns. The TBWP of the generated LCMW is estimated to be around 95.54. Fig. 9(c) shows the compressed pulse with a pulse width of 48 ps, and a pulse compression ratio as large as 141.8 is obtained. Since the both LC-WBGs are reverse biased, their chirp rates are both increased, which leads to a smallest chirp rate of the generated LCMW and a smallest TBWP.

Finally, a reverse biased voltage of +20 V is applied to the LC-WBG in the upper arm and a forward biased voltage of 1.0 V is applied to the LC-WBG in the lower arm. Fig. 10(a) shows the temporal waveform of the generated LCMW. As can be seen, the generated LCMW has a temporal duration of around 9.05 ns. Fig. 10(b) presents its spectrogram which exhibits a symmetrical chirp profile and a central frequency of 0.79 GHz. On the right side of the center, the instantaneous frequency is linearly increasing with a positive chirp rate of 2.82 GHz/ns. On the left side of the center, the instantaneous frequency is linearly decreasing with a negative chirp rate of -6.05 GHz/ns. The TBWP of the generated LCMW is estimated to be around 142.6. Fig. 10(c) shows the compressed pulse with a pulse width of 45 ps, and a pulse compression ratio as large as 191.0 is obtained. The LC-WBG with a forward biased voltage has a

smaller chirp rate, which counteracts the result caused by the LC-WBG with a reverse biased voltage.

If two identical bias voltages of -1.0 V are applied to the two LC-WBGs, due to an increase in the insertion losses induced by the increased free-carrier density, the optical performance of the spectral shaper is heavily degraded. Although only four bias voltage pairs are selected in the experiment to generate four chirped microwave waveforms, the results can be extended to generate any chirped microwave waveform when the bias voltages are continuously tuned. In addition, in the proposed electrically-tunable spectral shaper, a symmetrical interferometer structure is employed, which leads to the generated LCMW to have a symmetrical chirp profile in its spectral response and a zero frequency in the center of the generated LCMW. It is convenient to add an offset waveguide in one of the arms to introduce a non-zero length difference between the two arms, which could result in a monotonous chirp profile and a nonzero frequency in the generated LCMW. Furthermore, significant sidelobes are observed in the compressed pulse. In theory, a LCMW with a rectangular spectral profile would lead to a Sinc-type compressed pulse [23]. For our generated LCMWs, they have an approximately rectangular spectral profile. This is the reason why the sidelobes are large after pulse compression. By modifying the spectrum of an LCMW to have a bell-shaped profile, the sidelobes could be reduced. This can be done by applying apodization to the grating.

It is a big challenge in fabricating accurately the electrically-tunable LC-WBGs in the spectral shaper using the 248-nm process due to the lithography smoothing effect. The tuning efficiency of the LC-WBGs and the optical performance of the spectral shaper could be improved by optimizing the grating strength, the PN junction design, and the fabrication process.

V. CONCLUSION

A silicon-based on-chip electrically-tunable spectral shaper was designed, fabricated and its use for tunable LCMW generation based on SS-WTT mapping was demonstrated. The on-chip spectral shaper has a Michelson interferometer structure with two electrically-tunable LC-WBGs incorporated in its two arms. The spectral response of the spectral shaper exhibited a symmetrical, linearly increasing, or linearly decreasing FSR, which was required for the generation of a LCMW based on SS-WTT mapping. To enable the spectral shaper to have an electrically-tunable spectral response, a lateral PN junction was introduced to each of the two LC-WBGs. Due to the plasma dispersion effect, the spectral response of an LC-WBG could be tuned by tuning the bias voltage applied to the LC-WBG. The incorporation of two LC-WBGs into the interferometer led to a spectral shaper with a tunable spectral response. The proposed on-chip spectral shaper was fabricated using a CMOS-compatible process with 248-nm deep ultraviolet lithography and its use for tunable LCMW generation was demonstrated. The key advantage of using the spectral shaper for LCMW generation is the ultra-fast electrical tuning of the generated LCMW due to the ultra-fast plasma dispersion effect, which is in a scale of nanoseconds.

ACKNOWLEDGMENT

The authors would like to thanks CMC Microsystems, for providing the design tools and enabling the fabrication of the device.

REFERENCES

- [1] D. K. Barton, *Radar System Analysis and Modeling*. Boston, MA, USA: Artech House, 2005.
- [2] A. W. Rihaczek, *Principles of High-Resolution Radar*. Boston, MA, USA: Artech House, 1996.
- [3] H. D. Griffiths and W. J. Bradford, "Digital generation of high time bandwidth product linear FM waveforms for radar altimeters," *IEE Proc. Radar Signal Process.*, vol. 139, no. 2, pp. 160–169, Apr. 1992.
- [4] H. Kwon and B. Kang, "Linear frequency modulation of voltage controlled oscillator using delay-line feedback," *IEEE Microw. Wireless Compon. Lett.*, vol. 15, no. 6, pp. 431–433, Jun. 2005.
- [5] J.-W. Shi *et al.*, "Photonic generation and wireless transmission of linearly/nonlinearly continuously tunable chirped millimeter-wave waveforms with high time-bandwidth product at W-band," *IEEE Photon. J.*, vol. 4, no. 1, pp. 215–223, Feb. 2012.
- [6] A. Zeitouny, S. Stepanov, O. Levinson, and M. Horowitz, "Optical generation of linearly chirped microwave pulses using fiber Bragg gratings," *IEEE Photon. Technol. Lett.* vol.17, no. 3, pp. 660–662, Mar. 2005.
- [7] J. D. McKinney, D. E. Leaird, and A. M. Weiner, "Millimeter-wave arbitrary waveform generation with a direct space-to-time pulse shaper," *Opt. Lett.*, vol. 27, no. 15, pp. 1345–1347, Aug. 2002.
- [8] H. Gao *et al.*, "A simple photonic generation of linearly chirped microwave pulse with large time-bandwidth product and high compression ratio," *Opt. Express*, vol. 21, no. 20, pp. 23107–23115, Oct. 2013.
- [9] C. Wang and J. P. Yao, "Large time-bandwidth product microwave arbitrary waveform generation using a spatially discrete chirped fiber Bragg grating," *J. Lightw. Technol.*, vol. 28, no. 11, pp. 1652–1660, Jun. 2010.
- [10] H. Zhang, W. Zou, and J. Chen, "Generation of a widely tunable linearly chirped microwave waveform based on spectral filtering and unbalanced dispersion," *Opt. Lett.*, vol. 40, no. 6, pp. 1085–1089, Mar. 2015.
- [11] J. P. Yao, "Photonic generation of microwave arbitrary waveforms," *Opt. Commun.*, vol. 284, no. 15, pp. 3723–3736, Jul. 2011.
- [12] R. Ashrafi, Y. Park, and J. Azana, "Fiber-based photonic generation of high-frequency microwave pulses with reconfigurable linear chirp control," *IEEE Trans. Microw. Theory Technol.*, vol. 58, no. 11, pp. 3312–3319, Nov. 2010.
- [13] M. Li and J. P. Yao, "Photonic generation of continuously tunable chirped microwave waveforms based on a temporal interferometer incorporating an optically-pumped linearly-chirped fiber Bragg grating," *IEEE Trans. Microw. Theory Technol.*, vol. 59, no. 12, pp. 3531–3537, Dec. 2011.
- [14] A. Rashidinejad and A. M. Weiner, "Photonic radio-frequency arbitrary waveform generation with maximal time-bandwidth product capability," *J. Lightw. Technol.*, vol. 32, no. 20, pp. 3383–3393, Oct. 2014.
- [15] D. Marpaung *et al.*, "Integrated microwave photonics," *Lasers Photon. Rev.*, vol. 7, no. 4, pp. 506–538, Jul. 2013.
- [16] W. Zhang and J. P. Yao, "Silicon-based integrated microwave photonics," *IEEE J. Quantum Electron.*, vol. 52, no. 1, Jan. 2016, Art. no. 0600412.
- [17] M. Khan *et al.*, "Ultrabroad-bandwidth arbitrary radiofrequency waveform generation with a silicon photonic chip-based spectral shaper," *Nature Photon.*, vol. 4, no. 2, pp. 117–122, Feb. 2010.
- [18] W. Zhang and J. Yao, "Photonic generation of linearly chirped microwave waveform with a large time-bandwidth product using a silicon-based on-chip spectral shaper," in *Proc. Int. Topical Meeting Microw. Photon.*, Paphos, Cyprus, Oct. 2015, pp. 1–4.
- [19] W. Zhang and J. Yao, "Photonic generation of linearly chirped microwave waveforms using a silicon-based on-chip spectral shaper incorporating two linearly chirped waveguide Bragg gratings," *J. Lightw. Technol.*, vol. 33, no. 24, pp. 5047–5054, Dec. 2015.
- [20] H. Yun, W. Shi, Y. Wang, L. Chrostowski, and N. Jaeger, "2 × 2 adiabatic 3-dB coupler on silicon-on-insulator rib waveguides," *Proc. SPIE, Photonics North*, vol. 8915, pp. 89150V, May 2013.
- [21] Y. Wang, J. Flueckiger, C. Lin, and L. Chrostowski, "Universal grating coupler design," *Proc. SPIE, Photonics North*, vol. 8915, pp. 89150Y, May 2013.
- [22] X. Wang *et al.*, "Lithography simulation for the fabrication of silicon photonic devices with deep-ultraviolet lithography," in *Proc. IEEE Conf. Group IV Photon.*, San Diego, CA, USA, 2012, pp. 288–290.
- [23] J. Klauder, A. Price, S. Darlington, and W. Albersheim, "The theory and design of chirp radars," *Bell Syst. Tech. J.*, vol. 39, pp. 745–808, Jul. 1960.

Weifeng Zhang (S'12) received the B.Eng. degree in electronic science and technology from Xi'an Jiaotong University, Xi'an, China, in 2008, and the M.A.Sc. degree in electrical engineering from the Politecnico di Torino, Torino, Italy, in 2011. He is currently working toward the Ph.D. degree at Microwave Photonics Research Laboratory, School of Electrical Engineering and Computer Science, University of Ottawa, Ottawa, ON, Canada.

His current research interests include silicon photonics and its applications in microwave photonics.

Jianping Yao (M'99–SM'01–F'12) received the Ph.D. degree in electrical engineering from the Université de Toulon et du Var, Toulon, France, in December 1997. He is a Professor and University Research Chair in the School of Electrical Engineering and Computer Science, University of Ottawa, Ottawa, Ontario, Canada. From 1998 to 2001, he was with the School of Electrical and Electronic Engineering, Nanyang Technological University, Singapore, as an Assistant Professor. In December 2001, he joined the School of Electrical Engineering and Computer Science, University of Ottawa, as an Assistant Professor, where he became an Associate Professor in 2003, and a Full Professor in 2006. He was appointed as a University Research Chair in Microwave Photonics in 2007. From July 2007 to June 2010, he was the Director of the Ottawa-Carleton Institute for Electrical and Computer Engineering. He was reappointed as the Director of the Ottawa-Carleton Institute for Electrical and Computer Engineering in 2013.

He has authored or coauthored more than 510 research papers, including more than 300 papers in peer-reviewed journals and 210 papers in conference proceedings. He is a Topical Editor for *Optics Letters*, and serves on the Editorial Boards of the IEEE TRANSACTIONS ON MICROWAVE THEORY AND TECHNIQUES, *Optics Communications*, *Frontiers of Optoelectronics*, and *Science Bulletin*. He was as a Guest Coeditor for a Focus Issue on Microwave Photonics in *Optics Express* in 2013 and a Lead-Editor for a Feature Issue on Microwave Photonics in *Photonics Research* in 2014. He is a Chair of numerous international conferences, symposia, and workshops, including the Vice Technical Program Committee (TPC) Chair of the IEEE Microwave Photonics Conference in 2007, TPC Co-Chair of the Asia-Pacific Microwave Photonics Conference in 2009 and 2010, TPC Chair of the high-speed and broadband wireless technologies subcommittee of the IEEE Radio Wireless Symposium in 2009–2012, TPC Chair of the microwave photonics subcommittee of the IEEE Photonics Society Annual Meeting in 2009, TPC Chair of the IEEE Microwave Photonics Conference in 2010, General Co-Chair of the IEEE Microwave Photonics Conference in 2011, TPC Co-Chair of the IEEE Microwave Photonics Conference in 2014, and General Co-Chair of the IEEE Microwave Photonics Conference in 2015. He is also a Committee Member of numerous international conferences, such as IPC, OFC, BGPP, and MWP. He received the 2005 International Creative Research Award of the University of Ottawa. He received the 2007 George S. Glinski Award for Excellence in Research. In 2008, he received the Natural Sciences and Engineering Research Council of Canada Discovery Accelerator Supplements Award. He was selected to receive an inaugural OSA Outstanding Reviewer Award in 2012. He is currently an IEEE MTT-S Distinguished Microwave Lecturer for 2013–2015.

He is a registered Professional Engineer of Ontario. He is a Fellow of the Optical Society of America and the Canadian Academy of Engineering.